Analysis

Exploring mesoscopic mass transport effects on electrocatalytic selectivity

Hendrik H. Heenen ✉, Hemanth S. Pillai, Karsten Reuter & Vanessa J. Bukas ✉

Electrocatalytic selectivity is often discussed at the atomic level on the basis of the active site, while ignoring more subtle effects of mesoscopic mass transport. Here we show how transport controls selectivity through the exchange of surface-bound reaction intermediates between the electrode and bulk electrolyte. We argue that the arising kinetic competition changes with the catalyst's surface area and can become relevant for technologically important reactions including, for example, different products during the electrochemical CO_2 reduction on Cu-based catalysts. Combining microkinetic and transport modelling in a multi-scale approach, we specifically explore and quantify this effect for various showcase examples in the experimental literature. Despite its simplicity, our model correctly reproduces selectivity trends with respect to catalyst roughness on all meso-, micro- and atomic scales. The resulting insight provides an alternative or, at least, complementary explanation to changes in electrocatalytic selectivity that have otherwise been attributed to nano-structuring of active sites or electronic effects due to doping or alloying.

Heterogeneous electrocatalysis is at the heart of developing sustainable energy technologies. The rational design of more efficient electrocatalysts, however, hinges upon improving our fundamental understanding of the underlying reaction mechanisms. At the microscopic level, these mechanisms are currently almost exclusively discussed through the lens of the catalytically active site[1]. The emerging mechanistic picture is one that is entirely focused on surface-bound reaction intermediates and the simple assumption that catalytic rates are directly controlled through the adsorption strength of these intermediates. Subsequent catalyst design strategies therefore revolve around tuning the nature of the active site, for example, through doping or alloying. This approach has been met with tremendous success in predicting activity trends across different catalysts in computational screening studies, for example, the electrochemical oxygen reduction reaction (ORR)[2–4], CO_2 reduction reaction (CO2RR)[5–7] and many others[1]. It has been known to fail, however, when it comes to more subtle aspects of the electrochemical kinetics. Such aspects can be decisive in determining the reaction path that is being followed and thus the final product that is being formed. Increasing experimental evidence, for example, shows electrocatalytic selectivity change with catalyst loading or

reactor design in a non-obvious way that cannot be simply rationalized through considerations of the active site and its immediate chemical environment. Such puzzling effects bring the active site model into perspective and suggest a possibly important mechanistic role for mesoscopic mass transport phenomena[8,9].

Mesoscopic mass transport can influence electrocatalytic processes in different ways. Diffusion limitations of reactants/products as well as so-called local pH and other ion effects are gaining increasing attention[8,10–19], especially in light of the urgent drive to up-scale electrochemical process designs in recent years. We will focus here, however, on a considerably less-studied effect of mass transport: the kinetic competition that arises from exchanging volatile reaction intermediates between the electrocatalyst surface and bulk electrolyte. This reaction model was first proposed by Behm et al. and coined the desorption–re-adsorption–reaction mechanism[20–22]. The basis for the underlying mechanism is the desorption of a specific surface-bound and usually closed-shell reaction intermediate, whose subsequent fate creates a bifurcation in the reaction pathway: either to re-adsorb onto the surface towards full conversion, or to entirely diffuse away and thus be detected as an early, partially converted product. Electrocatalytic

selectivity is thus driven by the competition between surface kinetics and diffusion. Given this competition, descriptors of a catalyst's morphology such as the catalyst loading or inter-particle distance become critical as they directly affect the probability of re-adsorption, that is, the probability that the diffusing species returns to the surface for continued reaction rather than escaping as an early intermediate product.

While largely overlooked, there have been some experimental reports recognizing the role of the desorption–re-adsorption–reaction mechanism in individual cases. In their original work, Behm et al. purposefully manipulated the catalyst loading to demonstrate how selectivity depends upon surface roughness during the ORR on Pt[22] as well as the electrochemical oxidations of methanol (MOR)[20] and ethanol (EOR)[21]. More recently, similar mechanistic arguments were made to explain the varying selectivity towards CO during the CO_2RR on Cu when changing the catalyst morphology (via, for example, nanoparticle coverage, distance, shape and size)[23–25] or the reactant stream in reactor setups[26–28]. And yet, the impact of the desorption–re-adsorption–reaction mechanism as well as its generalization across different processes and systems remain unclear.

In this Analysis, we demonstrate the role of mesoscopic mass transport in determining electrocatalytic selectivity for a number of technologically important processes, including the ORR and different products of CO_2RR on Cu. Quantitative understanding of the underlying desorption–re-adsorption–reaction mechanism is established, by developing a simple multi-scale model that couples diffusion to the electrochemical surface kinetics. Our model correctly reproduces a series of trends found in the experimental literature, while providing an alternative or, at least, complementary explanation to changes in electrocatalytic selectivity beyond the active site model. Within this picture, the electrode surface roughness emerges as a descriptor of selectivity that effectively captures the influence of catalyst morphology across multiple length scales: the mesoscopic scale at the inter-particle level, microscopic scale at the intra-particle level and nanoscopic scale at the atomic level. Our analysis finally highlights the relevance of the desorption–re-adsorption–reaction mechanism in catalyst degradation as morphological changes over time (for example, due to nanoparticle agglomeration) induce corresponding changes in electrocatalytic selectivity.

A kinetic model for the desorption– re-adsorption–reaction mechanism

The desorption–re-adsorption–reaction mechanism describes the fate of a specific surface-bound, yet volatile, intermediate along the reaction path. The mechanism is schematically illustrated in Fig. 1 where this key intermediate X* (asterisk denotes an adsorbed configuration) faces a branching in the reaction path to either continue along the potential-dependent surface route towards full catalytic conversion (1) or desorb above the surface where it starts to build up a local concentration gradient (2). In the second case, if diffusion is fast enough, the near-surface species X(*) will leave the surface entirely and be detected as an early partially converted product X(aq) in the bulk (aqueous) solvent. If diffusion is relatively slow, however, X(*) faces the prospect of re-adsorbing onto the surface where it will once again be subjected to the (1) versus (2) competition described above. The mechanism thus essentially boils down to a competition between surface kinetics and diffusion. To describe this competition, we couple these two key components within a simple kinetic model of the selectivity-determining step.

We describe the surface reaction steps through a mean-field microkinetic model, while mass transport is simply included as one-dimensional Fickian diffusion (in the direction perpendicular to the surface). The two model components are then coupled via the flux of species X(*) and we solve the problem iteratively for steady-state solutions. In practice, the steady-state assumption reduces the transport modelling to a simple analytical expression of Fick's first law[29].

A converged solution is one where the diffusion flux J_{diff} of species X(*) equals the corresponding flux output from the microkinetic model J_{mkm} (= turnover frequency × active site density) after normalizing the rate to account for the density of catalytically active sites:

$$\frac{J_{mkm}}{J_{diff}} = \rho := \frac{A_{ECSA}}{A_{geo}} \tag{1}$$

Here, the normalizing factor ρ represents the catalyst roughness, defined as the ratio of the electrochemically active surface area (A_{ECSA}) to the geometric surface area (A_{geo}) of the electrode. Roughness thus enters the model as a central key parameter, designed to effectively capture the influence of catalyst morphology on the resulting product selectivity. Importantly, as a commonly measurable quantity (for example, through capacitive charging or measured current densities), this parameter ρ also allows us to draw a direct relation to experimental trends in the following.

Apart from the electrocatalyst roughness, we include six additional parameters in our model. Three of these parameters enter the microkinetic model as the activation free energies for each of the competing surface reaction steps: the redox barrier $\Delta G^{\ddagger}_{rdx}(U)$ for further electrocatalytic conversion of X* at the surface, the barrier $\Delta G^{\ddagger}_{des}$ for X* desorption and the reverse barrier $\Delta G^{\ddagger}_{ads}$ for X(*) adsorption. Among these barriers, we assume that only $\Delta G^{\ddagger}_{rdx}$ depends on the applied electrode potential U, while desorption/adsorption are treated as purely chemical steps and thus entirely independent of potential. This assumption needs to be treated with some caution as it is well known that also adsorption/desorption steps will change with potential depending upon the strength of the adsorbate's dipole moment or electrosorption valency, see for example, refs. 30,31. It is nevertheless an important distinction to make as it suggests that U can change selectivity by shifting the competition towards or against the surface redox reaction[9,32]. Again, this is a dependence that we will rely upon in the following when comparing against experimental selectivity data. Finally, the remaining three model parameters are part of the transport modelling: the diffusion coefficient D_{diff} and diffusion length L_{diff} of species X(*) (which simplify the otherwise complex hydrodynamic dimensionless constants), as well as Henry's solubility constant H_s, which is used to convert between activity and concentration. Further details on our kinetic model can be found in Supplementary Methods. At this point, it should be emphasized that the presented approach is focused on the transport of reaction intermediates without considering other mesoscopic effects that are at play at the electrochemical double layer. A more comprehensive evaluation of these multiple factors can, for example, be included via a modified Poisson–Nernst–Planck model, coupled to the potential-dependent surface reaction kinetics[16,18]. Such approaches have shown great promise in describing local pH effects[19] and the mechanistic role of electrolyte ions[15–17], as well as the influence of surface morphology on the local electric field that drives the catalysis[18].

Screening the above model parameters allows to explore their effect on selectivity within the desorption–re-adsorption–reaction mechanism. Our sensitivity analysis (Supplementary Methods) shows the most dramatic, exponential dependence coming from the competing reaction barriers $\Delta G^{\ddagger}_{rdx}(U)$, $\Delta G^{\ddagger}_{des}$ and $\Delta G^{\ddagger}_{ads}$, as well as from the electrode potential U (indirectly through $\Delta G^{\ddagger}_{rdx}$). This exponential dependence follows that of the resulting reaction rates and can change the selectivity towards X(aq) from 100% to 0% within only few hundred millivolts of increasing overpotential (Supplementary Fig. 2). In comparison, the effect from varying catalyst morphology is weaker and emerges as an asymptotic $1/\rho$ dependence in selectivity. This relation is founded in the competition between diffusion and re-adsorption: the probability of X(*) re-adsorption increases linearly with ρ, thus leading to more of the final product and less of the volatile intermediate product. Albeit weaker than the dramatic response to U, the role of ρ
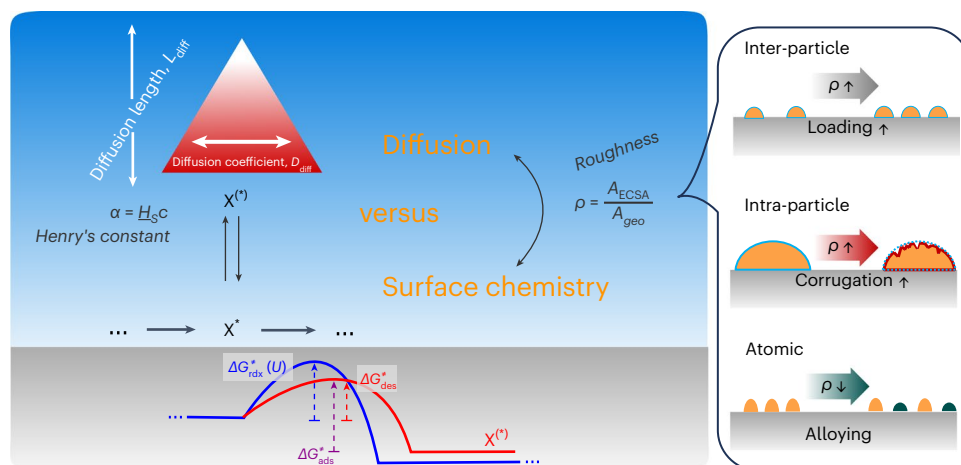
Fig. 1 | Schematic representation of the desorption–re-adsorption–reaction mechanism. A surface-bound, closed-shell intermediate X* faces the kinetic competition between a forward surface redox step versus desorption. Following desorption, if diffusion is fast enough, near-surface X$^{(*)}$ species will escape into the bulk electrolyte and be detected as an early, partially converted product. Our model couples diffusion with the surface kinetics via the surface roughness ρ, which effectively captures the influence of catalyst morphology across multiple length scales: at the inter-particle (for example via catalyst loading), intra-particle (for example via microscopic surface roughening) and atomic (via surface alloying) levels. Additionally shown are the other six parameters entering our model: free-energy barriers ($\Delta G_{rdx}^{\ddagger}(U)$, $\Delta G_{des}^{\ddagger}$ and $\Delta G_{ads}^{\ddagger}$), as well as diffusion-related properties (D_{diff}, L_{diff} and H_s) as described in the text.

can still be crucial to catalytic performance as will be demonstrated in the following. Finally, when chosen within physically reasonable ranges (Supplementary Fig. 2), the remaining transport-related parameters (D_{diff}, L_{diff} and H_s) generally influence selectivity to a much lesser extent. For example, exchanging the D_{diff} value of acetaldehyde (13.75×10^{-10} m² s⁻¹) to that of CO (20.3×10^{-10} m² s⁻¹) will typically only increase selectivity towards the diffusing intermediate product by <10%.

In the following, we focus on ρ and (to a second extent) U as variables against which to predict selectivity for several showcase catalytic reactions. As already indicated, the reasons for this choice include the strong influence of these two parameters on selectivity with asymptotic and exponential behaviours, respectively, according to $\propto \frac{\exp(-U)}{\rho}$, as well as the ability to draw a direct connection to measurable experimental variables. The remaining model parameters are then either taken from the literature or approximated to fit experiment (Supplementary Methods). Values for the activation free energies in particular, as well the potential-dependent $\Delta G_{rdx}^{\ddagger}(U)$ functional form, are unfortunately mostly unavailable and are thus fitted to reproduce measured selectivity curves. It is important to stress, however, that the effect of ρ in these situations is always simulated by consistently re-using the same set of parameters within each reaction model studied. This allows for an unbiased comparison of the results when specifically focusing on the response to varying catalyst morphology.

Selectivity changes with electrocatalyst morphology

In the following sections we explore the effect of catalyst morphology as it arises from surface roughening on different length scales: the inter-particle, intra-particle and atomic levels.

The effect of catalyst loading

We first consider selectivity as a function of catalyst coverage or loading on the electrode support. This effect corresponds to catalyst roughening at the particle level and has been systematically investigated by the group of Behm for different electrocatalytic reactions on Pt electrodes. Figure 2 shows digitized data from two such experimental studies for the ORR on polycrystalline (PC) Pt discs[22] (Fig. 2a) and MOR on Pt nanoparticles[20] (Fig. 2b). Both of these reactions involve volatile intermediates that may give rise to early, partially converted products
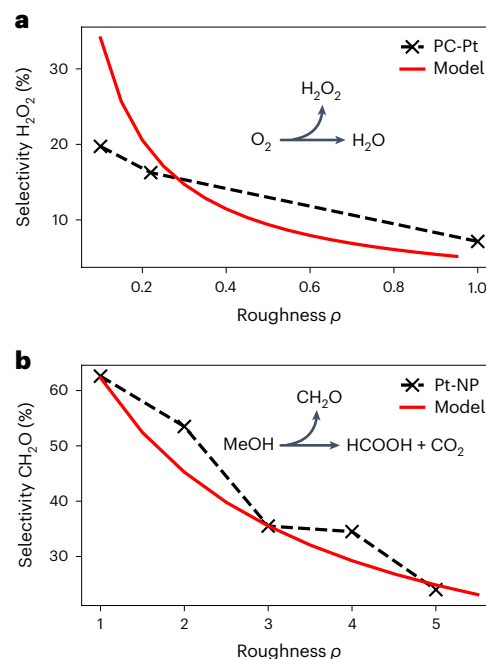
Fig. 2 | Selectivity changes with electrocatalyst roughness due to particle loading. a,b, Selectivity towards the early, partially converted products H₂O₂ during the ORR (**a**) and CH₂O during MOR (**b**), as a function of catalyst roughness ρ. Solid red lines show predictions from our kinetic model, while black `x' markers represent experimental data adapted from refs. 22 and 20, respectively. The dashed lines are meant to guide the eye. Experimental catalyst morphologies are PC Pt discs for which we reference ρ against a planar ($\rho = 1$) electrode surface (**a**) and Pt nanoparticles (NP) where we normalize ρ by the measured catalyst mass (**b**). The ORR data are measured at 0.58 V versus the reversible hydrogen electrode (RHE), while the MOR data are collected in the 0.16–1.16 V versus RHE range. All experiments were performed in 0.5 M sulfuric acid. For further details, cf. Supplementary Note 2.

following the desorption–re-adsorption–reaction mechanism. We therefore want to examine the yield towards these early products versus all later products that can appear further down the reaction

path: hydrogen peroxide (H_2O_2) versus water in the case of ORR, and formaldehyde (CH_2O) versus formic acid (HCOOH) plus CO_2 in the case of MOR (Supplementary Note 1). It is exactly this selectivity that is plotted in Fig. 2a,b, respectively, as a function of the electrocatalyst roughness ρ. The roughness parameter was purposefully manipulated during these experiments by carefully controlling the Pt catalyst loading and is measured here either against a planar electrode surface (for which $\rho = 1$ is assumed) in Fig. 2a or normalized by mass (such that $\rho = 1$ corresponds to the lowest mass loading experiment of 7 µg cm^{-2} Pt) in Fig. 2b. Either way, the resulting data clearly show that catalyst roughening decreases the selectivity towards the early, partially converted (H_2O_2 or CH_2O) product.

The mechanistic picture emerging from the two case studies shown in Fig. 2 is perfectly consistent with the desorption–re-adsorption–reaction mechanism. Following the rationale provided by Behm et al., higher catalyst loading means smaller distance between neighbouring particles and thus a higher probability for diffusing intermediates to re-adsorb. More re-adsorption favours continued surface reaction and lowers the selectivity towards the partially converted product. Considering its simplicity, our kinetic model captures this effect with almost remarkable agreement to experiment. The theoretical predictions (using model parameters listed in Supplementary Table 2) are represented by the solid red lines in Fig. 2 and show the anticipated $1/\rho$ dependence discussed in the previous section. These curves largely reproduce the experimental trends. Deviation is most noticeable only under conditions of ultralow catalyst loading ($\rho < 0.2$) in Fig. 2a. The model's over-estimation of the experimental H_2O_2 selectivity may be attributed to an inhomogeneous distribution of catalyst particles that cannot be described by our effective, one-dimensional ρ descriptor. The experiment–theory comparison is probably further skewed here by a more complex dependence on the applied electrode potential than that predicted by the desorption–re-adsorption–reaction mechanism (Supplementary Methods). This potential dependence has been previously discussed for the Pt-based ORR as the result of multiple competing reaction paths (that do not go through the volatile H_2O_2 intermediate)[22], but such mechanistic intricacies go well beyond the scope of our simple model and are not further discussed.

The effect of catalyst particle shape and surface corrugation

We next explored selectivity with varying catalyst particle shape and surface corrugation, that is, the influence of morphological features on the mesoscopic/microscopic range. These effects are demonstrated here for the CO_2RR on Cu electrodes, a model system of immense technological importance due to its unique ability to synthesize both a variety of one-carbon (C_1), but also high-value multi-carbon (C_{2+}) products. A study by the group of Jaramillo et al. identified and enumerated a total of 16 different possible products[33], of which we classify about half as the closed-shell intermediates that may be relevant to the desorption–re-adsorption–reaction mechanism. It is this intricate reaction network, along with the plethora of available experimental data, that make Cu-based CO_2RR an ideal playground to explore the effects of mass transport on electrocatalytic selectivity. In this section, we specifically focus on two such intermediates in the reaction mechanism: CO as the prominent first product following CO_2 electroreduction[34] and acetaldehyde (MeCHO), which appears further down the reaction path and competes with various other C_{2+} products[35–38].

Figure 3 compiles selectivity data from different experimental studies with very different catalyst morphologies. A Cu(111) single crystal[39], PC Cu foil (PC-Cu)[33], as well as two sets of data for oxygen-derived Cu (OD-Cu)[39,40] are all included in Fig. 3a, which plots the selectivity towards CO (versus all later C_1 plus C_{2+} products) as a function of the applied electrode potential U_{SHE} (referenced against the standard hydrogen electrode, SHE). All datasets for the different Cu catalysts are found to show a very similar exponential drop ($\propto \exp(-U_{SHE})$) in CO selectivity with increasingly reducing potentials.
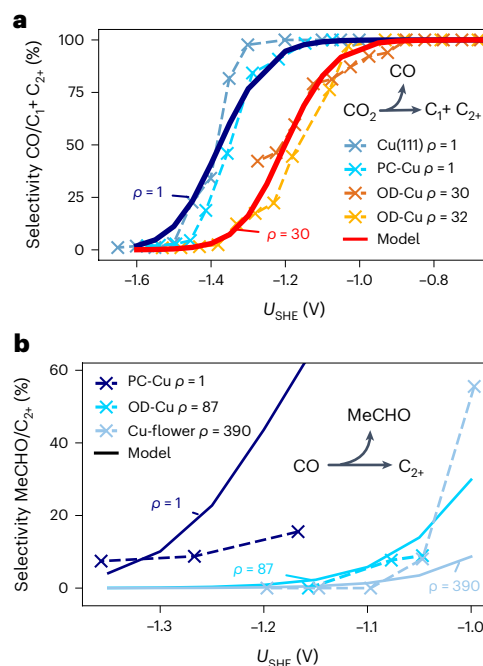
Fig. 3 | Selectivity changes with electrocatalyst particle shape and surface corrugation. a,b, Selectivity towards CO versus later C_1/C_{2+} products (**a**) and MeCHO versus later C_{2+} products (**b**) as a function of applied U_{SHE} potential during the CO_2RR on different Cu catalysts. The solid lines show theoretical predictions when varying only the roughness parameter ρ within each of the (CO and MeCHO) kinetic models. All 'x' markers represent experimental data adapted from (**a**) refs. 33,39,40 and (**b**) refs. 35,41,42. The dashed lines are meant to guide the eye. Experimental ρ values are assigned on the basis of measured (total) current densities, as marked in the figure's legend, with $\rho = 1$ for PC Cu as reference. All data were obtained in comparable H-cell setups in (**a**) 0.1 M KHCO$_3$ electrolyte and (**b**) a CO sparged 0.1 M KOH electrolyte, respectively. For further details, cf. Supplementary Note 2.

This effect can be simply explained on the basis of the desorption–re-adsorption–reaction mechanism: more reducing U_{SHE} drives forward the surface redox reaction, thus lowering the fraction of CO that desorbs and diffuses away. Using measured (total) current densities, we assign roughness values to the various Cu catalyst morphologies (Supplementary Notes 1 and 2) and thus reveal a second very important trend. Based on their corresponding roughness, we find that the presented CO selectivity curves are sorted into two distinct groups: Cu(111) and PC-Cu datasets with $\rho \approx 1$ fall pretty much on top of one another, implying essentially the same electrocatalytic behaviour due to surface restructuring under reaction conditions. With a higher ρ of about 30, however, the two curves representing the OD-Cu samples are clearly offset towards higher (less reducing) potentials. Again, in context of the desorption–re-adsorption–reaction mechanism, higher roughness means more re-adsorption and continued electrocatalytic conversion. As a result, at the same U_{SHE} value, OD-Cu has a lower affinity towards CO and higher affinity towards high-value C_{2+} products. Our kinetic model (Fig. 3a, solid lines) establishes this mechanistic picture. Using the exact same set of model parameters for all Cu catalysts (Supplementary Table 2) and varying only the ρ value between 1 and 30, reproduces the experimental offset between the two groups within semi-quantitative agreement.

The generality of the desorption–re-adsorption–reaction mechanism is further strengthened by our second case study in Fig. 3b, which plots the selectivity towards MeCHO (versus later C_{2+} products) as a function of U_{SHE}, while similarly compiling experimental data on different Cu morphologies: a PC-Cu sample of $\rho = 1$ (ref. 41), an OD-Cu

sample of ρ = 87 (ref. [35]) and a highly porous Cu nanoflower (Cu-flower) of ρ = 390 (ref. [42]). The exponential drop of MeCHO selectivity with reducing potentials is not as clear here as in the previous example due to the limited U_{SHE} range of the available experimental data. This relation is nevertheless predicted by our kinetic model (Fig. 3b, solid lines), along with the inverse relation with respect to catalyst roughness. While quantitative experiment–theory agreement is certainly far from perfect, the underlying trends are clearly compatible. Taken together, Fig. 3 confirms the prevalent notion that copper's meso- or microscopic morphology is critical to the resulting CO_2RR selectivity. These effects have so far mostly been associated, however, with changes in the nature or population of active sites such as under-coordinated steps and kinks due to roughening[43–46].

The effect of alloying

Our next and final case study addresses the effect of alloying. Alloying is often exploited in catalyst design as a tool that allows to manipulate the electronic properties, and hence reactivity, of the active site. This concept was recently invoked to rationalize the increased selectivity towards acetate (Ac) that was measured during CO electroreduction (CORR) on two different Cu-based alloys, namely Cu-Pd (ref. [47]) and Cu-Ag (ref. [48]). The authors of both these studies in fact found that there exists an optimal alloying ratio for which maximal selectivity towards this C_2 product is reached (Supplementary Note 2). They explained this on the basis of active site binding strengths. We argue here that modifying the density of active sites within the desorption–re-adsorption–reaction mechanism provides again an alternative, or at least complementary, reasoning to explain the reported selectivity changes.

In a combined experiment–theory study, some of us recently proposed that the mechanism for forming Ac on Cu is very much in line with the desorption–re-adsorption–reaction mechanism[32]. The case of Ac is just slightly more complicated by the fact that it is not directly acetate, but ketene, that desorbs from the surface. This earlier intermediate is then attacked by OH^- ions in the electrolyte to finally form Ac via a solution reaction step. While this last step introduces an additional pH dependence (through the involvement of OH^-), the selectivity towards Ac is still driven by the competition between surface kinetics and diffusion. The resulting $1/\rho$ dependence on catalyst morphology thus provides a reasonable explanation for lower Ac yields measured on more roughened Cu electrodes[32,49,50]. Our present model thus suggests the inverse effect from Pd- or Ag-based alloying.

Alloying a Cu catalyst with Pd or Ag effectively lowers ρ (according to the definition in equation (1) and assuming the alloying component remains at the surface under reaction conditions[51]) due to the lower density of catalytically active sites, at least of those sites that are selective towards forming the late C_{2+} products against which we measure here. This relation is best illustrated in Fig. 4, which compares different Cu-based catalysts in terms of Ac selectivity (versus later C_{2+} products) and catalytically relevant surface roughness at a fixed (U_{SHE} = −1.7 V) potential. The markers represent the data from the two experimental studies with corresponding ρ values estimated from measured current densities (Supplementary Notes 1 and 2): Cu-Pd catalyst samples (including both atomically ordered inter-metallic 'o-CuPd' and disordered 'CuPd$_{x\%}$' alloyed structures)[47], as well as Cu-Ag samples ('CuAg$_{x\%}$' alloys)[48] are included with different alloying ratios. These data are characterized by a much lower ρ as compared with their corresponding (non-alloy) Cu_2O (ref. [47]) and (pure) Cu (ref. [48]) reference samples. The higher ρ generally comes with lower Ac selectivity and we specifically outline a $1/\rho$ behaviour, characteristic for the desorption–re-adsorption–reaction mechanism. This trend is well reproduced by the kinetic model[32] when only varying the ρ parameter and keeping all other parameters fixed (solid red line in Fig. 4). The emerging mechanistic picture is thus very simple as it reduces the effect of alloying to merely lowering ρ within the desorption–re-adsorption–reaction
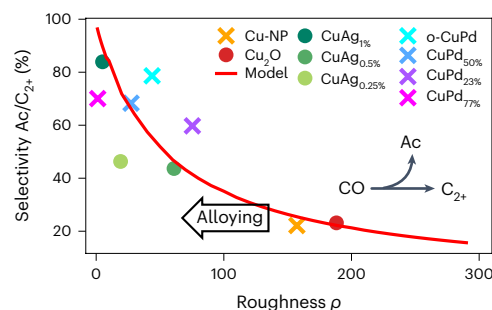
Fig. 4 | Selectivity changes with electrocatalyst roughness due to alloying. Selectivity towards acetate (Ac) versus later C_{2+} products during the CORR on different Cu-based catalysts, as a function of catalyst roughness ρ. Data are shown for a constant ($U_{SHE} \approx -1.7 \pm 0.03$ V) electrode potential. The solid red line shows the prediction of the kinetic model[32] when varying only the ρ parameter and keeping all other parameters fixed. The markers represent experimental data for Pd-based (crosses) and Ag-based (circles) Cu alloys with varying alloy ratios adapted from refs. [47] and [48], respectively. Additionally shown are data for an atomically ordered Cu-Pd inter-metallic (`o-CuPd') as well as pure Cu nanoparticles (NP)[47] and Cu_2O (ref. [48]) reference samples. All experimental ρ values are assigned on the basis of measured (total) current densities. For further details, cf. Supplementary Note 2.

model. One may therefore even think of alloying as changing the atomic-scale roughness. Lower ρ ultimately means that more Ac will escape as an intermediate species when measured against later, further-reduced C_{2+} products. We therefore suggest that high Ac selectivity is not necessarily unique to Cu-based alloys, but may be expected also on pure Cu electrodes if the surface morphology remains smooth enough under reaction conditions. There exists some experimental evidence to support this hypothesis[50,52]. Finally, generalizing this alloying effect, we note that similar observations have been made by the group of Koper and Jaramillo for the volatile products CO and acetaldehyde during the CO_2RR on Cu-Zn and Cu-Ag alloys, respectively[53,54].

Conclusions

This work calls attention to mesoscopic mass transport as a decisive factor in determining electrocatalytic selectivity. Through multi-scale modelling and a detailed inspection of the experimental literature, we quantify the effect of the so-called desorption–re-adsorption–reaction mechanism and show its generality over different redox reactions, different catalysts and different electrode setups. Importantly, our analysis highlights surface roughness as a key descriptor that can capture the effect of catalyst morphology on selectivity across all relevant length scales. This simple picture thus reduces into a (one-dimensional) roughness parameter any influence from morphology, regardless of its origin: catalyst loading, particle shape/size, surface corrugation due to, for example, oxidative pre-treatment or electro-polishing and even alloying. Since the suitability of this effective roughness descriptor may break down in certain situations[32], requiring, for example, an explicit two-dimensional consideration of surface corrugation, a systematic understanding of such cases is subject of ongoing work.

We believe the present mechanistic insight holds value for electrocatalyst design, not only towards optimizing steady-state operation, but also in the context of catalyst ageing and degradation. Roughness is, after all, most often a dynamic property under reaction conditions[55–58]. According to the desorption–re-adsorption–reaction mechanism, a dynamically evolving catalyst morphology (for example, due to reconstruction, particle agglomeration or dissolution) will change the resulting product selectivity and thus the targeted catalytic performance. We demonstrate this relation via, for example, time-dependent measurements during the CO_2RR on differently sized Cu nanoparticles[59]. Following the same procedure as above to extract roughness

estimates from experimental current densities, we find the expected trend for measured selectivity towards the intermediate CO product (Supplementary Note 3). Surface roughness decreases over time as Cu particles coalesce, and this leads to a simultaneous ca. 10–20% increase in CO selectivity already within the first 12 h of operation. A similar mechanistic picture emerges for the time-dependent selectivity towards H_2O_2 during the ORR on Pd (ref. 55) (Supplementary Note 3).

With the desorption–re-adsorption–reaction mechanism in mind, our final remark concerns system design strategies. In this study, we purposefully put focus on catalyst morphology and, to a second extent, the electrode potential as tunable parameters that can control product selectivity. Correspondingly, we also limited our literature search to laboratory-scale studies that usually rely on conventional H-cell or flow cell setups. While such setups leave little room for manipulating the electrolytes' macroscopic hydrodynamics, this situation changes when up-scaling towards the practical device level[26–28]. Here, careful reactor design to control the diffusion properties (captured by the diffusion length in our model) of volatile intermediates may prove particularly important to the resulting selectivity. Such effects have in fact already been demonstrated in designated reactors via rotation rates in rotating disc and rotating cylinder setups or flow rates in special flow cells, for example, for the selectivity of CO in CO_2RR[26–28] and for H_2O_2 in ORR on Pt (ref. 60) (see analysis in Supplementary Methods). In this context, unexplored effects due to special pore catalyst geometries[10,12] or particle arrangements[25] that go beyond our simplified one-dimensional transport model open up exciting research avenues.

Methods

Our kinetic model was developed as an in-house implementation. The surface kinetics are simulated via a mean-field model and solved for steady-state using an ordinary differential equation (ODE) solver available in the SciPy distribution[61]. Mass transport is included as one-dimensional diffusion and described analytically via Fick's first law[29]. A boundary condition is set by assigning the bulk concentration of desorbing species to zero. The coupled microkinetic and transport models are then solved iteratively such that the flux of volatile species is consistent within the two models, given a fixed normalizing factor that is set through the roughness ρ parameter. This procedure corresponds in practice to optimizing the activity or concentration of near-surface species that enter the microkinetic or transport model, respectively. A more detailed description of the model is provided in Supplementary Methods.

Data availability

The digitized experimental data used for reference in this study are provided as an additional Source data file. Source data are provided with this paper.

Code availability

The code for our kinetic model is available in the GitHub repository at https://github.com/hheenen/model_transport_selectivity. All input model parameters specifically used in this study are listed in Supplementary Table 2 and ref. 32.

References

1. Seh, Z. W. et al. Combining theory and experiment in electrocatalysis: Insights into materials design. *Science* **355**, eaad4998 (2017).
2. Nørskov, J. et al. Origin of the overpotential for oxygen reduction at a fuel-cell cathode. *J. Phys. Chem. B* **108**, 17886–17892 (2004).
3. Greeley, J. et al. Alloys of platinum and early transition metals as oxygen reduction electrocatalysts. *Nat. Chem.* **1**, 552–556 (2009).
4. Kulkarni, A., Siahrostami, S., Patel, A. & Nørskov, J. K. Understanding catalytic activity trends in the oxygen reduction reaction. *Chem. Rev.* **118**, 2302–2312 (2018).
5. Bagger, A., Ju, W., Varela, A. S., Strasser, P. & Rossmeisl, J. Electrochemical CO_2 reduction: a classification problem. *ChemPhysChem* **18**, 3266–3273 (2017).
6. Tran, K. & Ulissi, Z. W. Active learning across intermetallics to guide discovery of electrocatalysts for CO_2 reduction and H_2 evolution. *Nat. Catal.* **1**, 696–703 (2018).
7. Zhong, M. et al. Accelerated discovery of CO_2 electrocatalysts using active machine learning. *Nature* **581**, 178–183 (2020).
8. Kas, R. et al. Electrochemical CO_2 reduction on nanostructured metal electrodes: fact or defect? *Chem. Sci.* **11**, 1738–1749 (2020).
9. Govindarajan, N., Kastlunger, G., Heenen, H. H. & Chan, K. Improving the intrinsic activity of electrocatalysts for sustainable energy conversion: where are we and where can we go? *Chem. Sci.* **13**, 14–26 (2022).
10. Modestino, M. A., Hashemi, S. M. H. & Haussener, S. Mass transport aspects of electrochemical solar-hydrogen generation. *Energy Environ. Sci.* **9**, 1533–1551 (2016).
11. Burdyny, T. & Smith, W. A. CO_2 reduction on gas-diffusion electrodes and why catalytic performance must be assessed at commercially-relevant conditions. *Energy Environ. Sci.* **12**, 1442–1453 (2019).
12. Suter, S. & Haussener, S. Optimizing mesostructured silver catalysts for selective carbon dioxide conversion into fuels. *Energy Environ. Sci.* **12**, 1668–1678 (2019).
13. Guo, J. et al. Mass transport modifies the interfacial electrolyte to influence electrochemical nitrate reduction. *ACS Sustain. Chem. Eng.* **11**, 7882–7893 (2023).
14. Ma, M. et al. Local reaction environment for selective electroreduction of carbon monoxide. *Energy Environ. Sci.* **15**, 2470–2478 (2022).
15. Ringe, S. et al. Understanding cation effects in electrochemical co2 reduction. *Energy Environ. Sci.* **12**, 3001–3014 (2019).
16. Zhang, L., Cai, J., Chen, Y. & Huang, J. Modelling electrocatalytic reactions with a concerted treatment of multistep electron transfer kinetics and local reaction conditions. *J. Phys. Condens. Matter* **33**, 504002 (2021).
17. Huang, J., Li, M., Eslamibidgoli, M. J., Eikerling, M. & Groß, A. Cation overcrowding effect on the oxygen evolution reaction. *JACS Au* **1**, 1752–1765 (2021).
18. Li, F., Zhou, C. & Klinkova, A. Simulating electric field and current density in nanostructured electrocatalysts. *Phys. Chem. Chem. Phys.* **24**, 25695–25719 (2022).
19. Zhu, X., Huang, J. & Eikerling, M. pH effects in a model electrocatalytic reaction disentangled. *JACS Au* **3**, 1052–1064 (2023).
20. Jusys, Z., Kaiser, J. & Behm, R. Methanol electrooxidation over Pt/C fuel cell catalysts: dependence of product yields on catalyst loading. *Langmuir* **19**, 6759–6769 (2003).
21. Wang, H., Jusys, Z. & Behm, R. Ethanol electrooxidation on a carbon-supported Pt catalyst: reaction kinetics and product yields. *J. Phys. Chem. B* **108**, 19413–19424 (2004).
22. Seidel, Y. et al. Mesoscopic mass transport effects in electrocatalytic processes. *Faraday Discuss.* **140**, 167–184 (2009).
23. Mistry, H. et al. Tuning catalytic selectivity at the mesoscale via interparticle interactions. *ACS Catal.* **6**, 1075–1080 (2016).
24. Wang, X., Varela, A. S., Bergmann, A., Kühl, S. & Strasser, P. Catalyst particle density controls hydrocarbon product selectivity in CO_2 electroreduction on CuO_x. *ChemSusChem* **10**, 4642–4649 (2017).
25. Grosse, P. et al. Dynamic transformation of cubic copper catalysts during CO_2 electroreduction and its impact on catalytic selectivity. *Nat. Commun.* **12**, 6736 (2021).
26. Lim, C., Harrington, D. & Marshall, A. Effects of mass transfer on the electrocatalytic CO_2 reduction on Cu. *Electrochim. Acta* **238**, 56–63 (2017).

27. Jang, J., Rüscher, M., Winzely, M. & Morales-Guio, C. G. Gastight rotating cylinder electrode: toward decoupling mass transport and intrinsic kinetics in electrocatalysis. *AIChE J.* **68**, e17605 (2022).

28. Watkins, N. et al. Hydrodynamics change tafel slopes in electrochemical CO_2 reduction on copper. *ACS Energy Lett.* **8**, 2185–2192 (2023).

29. Cussler, E. L. *Diffusion: Mass Transfer in Fluid Systems* (Cambridge Univ. Press, 2009).

30. Dudzinski, A. M., Diesen, E., Heenen, H. H., Bukas, V. J. & Reuter, K. First step of the oxygen reduction reaction on au(111): a computational study of O_2 adsorption at the electrified metal/water interface. *ACS Catal.* **13**, 12074–12081 (2023).

31. Bergmann, N., Hörmann, N. G. & Reuter, K. Ab initio-based modeling of thermodynamic cyclic voltammograms: a benchmark study on Ag(100) in bromide solutions. *J. Chem. Theory Comput.* **19**, 8815–8825 (2023).

32. Heenen, H. H. et al. The mechanism for acetate formation in electrochemical $CO_{(2)}$ reduction on Cu: selectivity with potential, pH, and nanostructuring. *Energy Environ. Sci.* **15**, 3978–3990 (2022).

33. Kuhl, K. P., Cave, E. R., Abram, D. N. & Jaramillo, T. F. New insights into the electrochemical reduction of carbon dioxide on metallic copper surfaces. *Energy Environ. Sci.* **5**, 7050–7059 (2012).

34. Hori, Y. in *Modern Aspects of Electrochemistry* 89–189 (Springer, 2008).

35. Bertheussen, E. et al. Acetaldehyde as an intermediate in the electroreduction of carbon monoxide to ethanol on oxide-derived copper. *Angew. Chem. Int. Ed.* **128**, 1472–1476 (2016).

36. Liu, X. et al. pH effects on the electrochemical reduction of $CO_{(2)}$ towards C_2 products on stepped copper. *Nat. Commun.* **10**, 32 (2019).

37. Kastlunger, G. et al. Using pH dependence to understand mechanisms in electrochemical co reduction. *ACS Catal.* **12**, 4344–4357 (2022).

38. Kastlunger, G., Heenen, H. H. & Govindarajan, N. Combining first-principles kinetics and experimental data to establish guidelines for product selectivity in electrochemical CO_2 reduction. *ACS Catal.* **13**, 5062–5072 (2023).

39. Huang, Y., Handoko, A. D., Hirunsit, P. & Yeo, B. S. Electrochemical reduction of CO_2 using copper single-crystal surfaces: effects of CO* coverage on the selective formation of ethylene. *ACS Catal.* **7**, 1749–1756 (2017).

40. Li, C. W. & Kanan, M. W. CO_2 reduction at low overpotential on Cu electrodes resulting from the reduction of thick Cu_2O films. *J. Am. Chem. Soc.* **134**, 7231–7234 (2012).

41. Bertheussen, E. et al. Electroreduction of CO on polycrystalline copper at low overpotentials. *ACS Energy Lett.* **3**, 634–640 (2018).

42. Wang, L. et al. Electrochemically converting carbon monoxide to liquid fuels by directing selectivity with electrode surface area. *Nat. Catal.* **2**, 702–708 (2019).

43. Jiang, K. et al. Effects of surface roughness on the electrochemical reduction of CO_2 over Cu. *ACS Energy Lett.* **5**, 1206–1214 (2020).

44. De Gregorio, G. L. et al. Facet-dependent selectivity of Cu catalysts in electrochemical CO_2 reduction at commercially viable current densities. *ACS Catal.* **10**, 4854–4862 (2020).

45. Rossi, K. & Buonsanti, R. Shaping copper nanocatalysts to steer selectivity in the electrochemical CO_2 reduction reaction. *Acc. Chem. Res.* **55**, 629–637 (2022).

46. Gauthier, J. A., Stenlid, J. H., Abild-Pedersen, F., Head-Gordon, M. & Bell, A. T. The role of roughening to enhance selectivity to C_{2+} products during CO_2 electroreduction on copper. *ACS Energy Lett.* **6**, 3252–3260 (2021).

47. Ji, Y. et al. Selective CO-to-acetate electroreduction via intermediate adsorption tuning on ordered Cu–Pd sites. *Nat. Catal.* **5**, 251–258 (2022).

48. Dorakhan, R. et al. A silver–copper oxide catalyst for acetate electrosynthesis from carbon monoxide. *Nat. Synth.* **2**, 448—457 (2023).

49. Jouny, M., Luc, W. & Jiao, F. High-rate electroreduction of carbon monoxide to multi-carbon products. *Nat. Catal.* **1**, 748–755 (2018).

50. Luc, W. et al. Two-dimensional copper nanosheets for electrochemical reduction of carbon monoxide to acetate. *Nat. Catal.* **2**, 423–430 (2019).

51. Vinogradova, O. V., Reuter, K. & Bukas, V. J. Trends of Pd_3Au(111) alloy surface segregation in oxygen, carbon, and nitrogen environments. *J. Phys. Chem. C* **127**, 22060–22066 (2023).

52. Zhu, P. et al. Direct and continuous generation of pure acetic acid solutions via electrocatalytic carbon monoxide reduction. *Proc. Natl Acad. Sci. USA* **118**, e2010868118 (2020).

53. da Silva, A. H. M. et al. Electrocatalytic CO_2 reduction to C_{2+} products on Cu and Cu_xZn_y electrodes: effects of chemical composition and surface morphology. *J. Electroanal. Chem.* **880**, 114750 (2021).

54. Wang, L. et al. Selective reduction of CO to acetaldehyde with CuAg electrocatalysts. *Proc. Natl Acad. Sci. USA* **117**, 12572–12575 (2020).

55. Mittermeier, T., Weiß, A., Gasteiger, H. A. & Hasché, F. Monometallic palladium for oxygen reduction in pem fuel cells: particle-size effect, reaction mechanism, and voltage cycling stability. *J. Electrochem. Soc.* **164**, F1081 (2017).

56. Karuppannan, M. et al. A highly durable carbon-nanofiber-supported Pt–C core–shell cathode catalyst for ultra-low pt loading proton exchange membrane fuel cells: facile carbon encapsulation. *Energy Environ. Sci.* **12**, 2820–2829 (2019).

57. Göhl, D. et al. Engineering stable electrocatalysts by synergistic stabilization between carbide cores and Pt shells. *Nat. Mater.* **19**, 287–291 (2020).

58. Kolle-Görgen, E., Fortunato, G. & Ledendecker, M. Catalyst stability in aqueous electrochemistry. *Chem. Mater.* **34**, 10223–10236 (2022).

59. Huang, J. et al. Potential-induced nanoclustering of metallic catalysts during electrochemical CO_2 reduction. *Nat. Commun.* **9**, 3117 (2018).

60. Marković, N. M., Gasteiger, H. A. & Ross, P. N. Oxygen reduction on platinum low-index single-crystal surfaces in alkaline solution:rotating ring disk$_{Pt(hkl)}$ studies. *J. Phys. Chem.* **100**, 6715–6721 (1996).

61. Virtanen, P. et al. Scipy 1.0: fundamental algorithms for scientific computing in Python. *Nat. Methods* **17**, 261–272 (2020).

Author contributions
H.H.H. and V.J.B. conceived the research project. H.H.H. developed the kinetic model and wrote the first draft of the manuscript. H.S.P. contributed to analysis and interpretation of the data, as well as literature review. K.R. contributed to the conceptual discussion. V.J.B. wrote the paper with input from all authors.

Competing interests

The authors declare no competing interests.

Additional information